# Supporting information:

# Post Gold King Mine spill investigation of metal stability in water and sediments of the Animas River watershed

*Lucia Rodriguez-Freire[1], Sumant Avasarala[1], Abdul-Mehdi S. Ali[2], Diane Agnew[3], Joseph H. Hoover[4], Kateryna Artyushkova[5], Drew E. Latta[6], Eric J. Peterson[5]; Johnnye Lewis[4]; Laura J. Crossey[2]; Adrian J. Brearley[2]; José M. Cerrato[1*]*

*Corresponding email address: jcerrato@unm.edu

Telephone: (001) (505) 277-0870

Fax: (001) (505) 277-1988

[1] Department of Civil Engineering, MSC01 1070, University of New Mexico, Albuquerque, New Mexico 87131, United States

[2] Department of Earth and Planetary Sciences, MSC03 2040, University of New Mexico, Albuquerque, New Mexico 87131, United States

[3] New Mexico Environment Department, 121 Tijeras Avenue NE, Albuquerque, New Mexico 87102, United States

[4] Community Environmental Health Program, MSC09 5360, University of New Mexico, Albuquerque, NM 87131, United States

[5] Department of Chemical and Biological Engineering, MSC01 1120, University of New Mexico, Albuquerque, New Mexico 87131, United States

[6] Department of Civil and Environmental Engineering, The University of Iowa, 4105 Seamans Center, Iowa City, Iowa 52242, United States

Journal: Environmental Science & Technology

Date: September 3, 2016

27 pages (including cover page)

8 Tables

7 Figures

## Table of Contents

## Iron speciation using Mössbauer spectra

**Animas River Sample C1.** The Mössbauer spectra of the Animas River Sediment C1 were collected and fit at temperatures of 77 K and 17.5 K (Figure 5A). At 77 K and 17.5 K the spectra can be modeled with 5 components (Table S7). The main component in the spectrum at both temperatures is a sextet with relative areas of 41.6% and 51.1%, at 77 K and 17.5 K, respectively, with Mössbauer parameters of center shift (CS) = 0.49 mm/s, quadrupole shift (QS) = -0.20 mm/s, and an average hyperfine field of 45.1 T at 17.5K (yellow sextet in Figure 5A). These Mössbauer parameters are consistent with those of nano-crystalline goethite.[1-3] In addition, at both temperatures a second sextet (red sextet in Figure 5A) is present (11.4% of the relative area at 17.5 K) with a lower QS of -0.14 mm/s and a higher average hyperfine field of 53.4 T consistent with the presence of weakly-ferromagnetic hematite that has not undergone the magnetic Morin transition even at 17.5 K.[1, 2] A lack of a Morin-transition in a natural hematite is not unexpected, and could be the result of small particle size and/or the presence of common impurities such as Al or Ti in the structure.[2,4]

Paragmagnetic Fe(III) is also present ($Fe^{3+}$ doublet 1 in Table S7, green doublet in Figure 5A) within the sample at both 77 K and 17.5, with parameters of CS = 0.49 mm/s and quadrupole splitting (QS) = 0.62-0.64 mm/s, which are consistent with any number of Fe(III) containing minerals, including primary silicates and clay minerals.[2, 5] The decrease in area of this component between 77 K and 17.5 K likely represents magnetic ordering of Fe(III) present as nano-crystalline goethite.[1] A second paramagnetic Fe(III) doublet ($Fe^{3+}$ doublet 2 in Table S7, purple doublet in Figure 5A) is also present, but the exact nature of this doublet with its Fe(III)-like CS (0.55 mm/s), and wide QS (1.83 mm/s) is unknown; however, some primary silicates

containing Fe(III) have large QS values at room temperature that are likely to be higher at 17.5 K.[5]

Finally, the spectrum also has a third doublet comprising 22.2 % of the relative area with a large CS and QS value (1.27, 2.83 mm/s) which can be assigned to paramagnetic octahedral Fe(II) in clay minerals, primary silicates, phosphates, and sulfates.[5] The Mössbauer parameters for the Fe(II) doublet are consistent with the XRD identification of chlorite and illite/mica type clay minerals.

**Animas River Samples L1 and L4.** As with sample C1, the Mössbauer spectra of the Animas River Sample L1 and L4 were collected and fitted at 77 K (Figure 5B and 5C). The Mössbauer hyperfine parameters derived from fitting are shown in Table S7. We have fit samples L1 and L4 with two doublets corresponding to Fe(II) and Fe(III), as well as several sextets. Fitting of a high CS and high QS component consistent with octahedral Fe(II) (CS = 1.26 mm/s, QS = 2.8 mm/s) shows that sample L4 has about 2-times as much Fe(II) (13.5% relative area compared to 6.6%). As noted above for the control sample, these hyperfine parameters are consistent with Fe(II) hyperfine parameters of multiple minerals and is not diagnostic of a single phase. Both samples have similar paramagnetic Fe(III) doublets at 77 K, with 35% and 40% of the total area, and similar hyperfine parameters of CS = 0.46-0.49 mm/s and QS = 0.83-0.88 mm/s. Between 77 K and 17.5 K the Fe(III) doublet (CS = 0.43 and 0.47 mm/s, respectively) decreases in area for both the samples, due to the magnetic ordering of Fe(III) within the samples to form sextets. At 17.5 K the Fe(III) doublets makes up 6.2 and 9.0 % of the area in samples L1 and L4, respectively, and have hyperfine parameters (CS = 0.43 and 0.47 mm/s, QS = 0.76 and 0.84 mm/s) consistent with octahedral Fe(III) in clay minerals, primary silicates, and phosphates.[5,6]

At 77K for samples L1 and L4 the major feature (59% and 45% for samples L1 and L4, respectively) is a sextet 77 K with hyperfine parameters consistent with those of nano-crystalline goethite (CS ≈ 0.48 mm/s, QS = -0.24 mm/s, and average hyperfine field (H) = 36 and 34 T, respectively).[1-3] The large standard deviation of the hyperfine field (σ(H), Tables S7), and the shoulder feature in the sextet suggest a large distribution in goethite particle sizes with a significant fraction present as nano-crystals.[1] In addition to the goethite sextet, sample L4 contains a smaller sextet (~2 %) consistent with weakly ferromagnetic hematite that has not undergone the Morin transition. The hyperfine parameters and magnetic behavior are consistent with those of the hematite in the control sample (discussed above).[1,2] At 17.5 K the spectral interpretation of the sextets in sample L1 and L4 are complicated by the appearance of a second major sextet with a lower average hyperfine field (orange fitting feature in Figure 5). Fitting of this feature reveals that it comprises the major proportion of the spectral area (70% in both samples). The Mössbauer parameters are similar to those of goethite (CS ≈ 0.48 mm/s, QS ≈ -0.2 mm/s), however both the hyperfine average hyperfine field (38 – 41 T) and quadrupole shift (QS = 2ε = -0.2 mm/s) are low compared to published values for nano-crystalline goethite[1] and that of the goethite at 77 K (QS = -0.24-0.26 mm/s). Based on XRD and TEM data suggesting the presence of jarosite, we can tentatively assign part of this sextet to jarosite.

Relatively little and conflicting information exists about the low temperature Mössbauer parameters of jarosite-group Fe-minerals, with conflicting reports of QS parameters of +0.25 to +0.55 mm/s[7] to -0.19 mm/s[3]. In order to resolve this discrepancy we synthesized the potassium form of jarosite,[8] confirmed its identity with XRD, and collected the Mössbauer spectrum at ~19 K (Figure S7A). The hyperfine parameters of this K-jarosite are CS = 0.49 mm/s, QS = 2ε = -0.16 mm/s, and H = 42.3 T. The synthetic jarosite parameters are consistent with those of the

lower QS and H sextet in samples L1 and L4. Furthermore, the high QS (0.83-0.88 mm/s) of the Fe(III) doublets of S2 and S5 would be consistent with a mixture of goethite (paramagnetic QS ≈ 0.55 mm/s[2] and higher QS jarosite with QS ≈ 1.13 mm/s (Figure S7A)). It is also likely that this sextet accounts for a significant fraction of the nanocrystalline goethite present, given the tendancy for lower average hyperfine fields and QS parameters in nano-goethite.[1,2]

Finally, to estimate the amount of jarosite present, we have fit the Mössbauer spectra collected at 270 K (Figure S7B, Table S7). At this temperature both samples L1 and L4 are primarily composed of (super-)paramagnetic Fe(III) and paramagnetic Fe(II) doublets, along with a collapsed sextet likely due to the presence of goethite and a sextet from hematite in L4. Two Fe(III) doublets are necessary to produce the best fits of the Mössbauer spectra of sample L1 and L4 at 270 K. One Fe(III) doublet has parameters (CS ≈ 0.4 mm/s, QS ≈ 0.5-0.6 mm/s) consistent with the parameters of super-paramagnetic goethite,[2] and the other has a higher QS value of ~1.0 to 1.1 mm/s, more consistent with that of jarosite near room temperature (Table S8).[9] Given the other evidence for jarosite, we suggest this doublet represents the jarosite present in the two samples. The fitting results suggest that 20-35% of the Fe present in the two samples is present as jarosite. Given the large error in the determined amounts (5-10 % of the total Fe), it not possible to assign a definitive difference between the two samples.

## Materials and methods

**Jarosite synthesis.** K-jarosite was used here due to the mild conditions required for synthesis compared to the hydrothermal conditions required for facile laboratory synthesis of hydronium-jarosite.[8] The jarosite here was synthesized according to the procedures in Dutrizac and Kaiman.[8] Briefly, 30 g/L of $KNO_3$ and 8 g/L of ferric sulfate (0.143 mole/L Fe(III)) were added to 250 mL of 0.01 M $H_2SO_4$ and heated for 1.5 h at 95 °C. The yellow precipitate was washed 3 times with

DI water by centrifugation and dried in an oven at 70 °C for 3 d. The powder X-ray diffraction pattern was consistent with that of the potassium form of jarosite.

**Anlytical techniques.** The total suspended metal concentration in water was measured after acidification of 30 ml of the unfiltered water samples using 3 ml hydrochloric acid, HCl, and 1 ml $HNO_3$. Sediment samples were dried overnight at 70 $^oC$ in a controlled–temperature oven, crushed, and homogenized prior to the analysis. Two grams of the pulverized sediment was digested with 6 ml HCl, and 2 ml $HNO_3$ and then heated in a Digi prep MS SCP Science block digester at 90 °C for 2 h. Sediment samples were then centrifuged for 10 min at 2,000 rpm to remove the residual undigested material, the supernatant was collect and the pellets were discarded. The sediment supernatant and the digested water samples were filtered through 0.45 μm filters (25 mm PTFE Membrane syringe filter) prior to any analyses. Sediment samples were additionally filtered using a 0.22 μm filters (10 mm PTFE Membrane syringe filter).

- A ThermoFisher Dionex Ion Chromatogram (IC) (ICS-1100) was used to analyze water samples for anion concentration
- Elemental composition of all samples was measured using Inductively Coupled Plasma ionization (ICP), coupled with either an Optical Emission Spectrometer (OES) or a Mass Spectrometer (MS):
    - OES: PerkinElmer Optima 5300DV Inductively Coupled Plasma-Optical Emission Spectrometer (ICP-OES) with a detection limit of < 0.01 mg $l^{-1}$.
    - MS: A PerkinElmer NexION 300D (Dynamic Reaction Cell) Inductively Coupled Plasma-Mass Spectrometer (ICP-MS), with a detection limit of < 0.5 μg $l^{-1}$ was used for trace element analysis

- Bulk sediment analysis was done by X-Ray Fluorescence with a Rigaku ZSX Primus II. For the XRF analysis, 9 g of the crushed sediments were combined with 1 g of SpectroBlend binder and compacted into a pellet.
- Sediments were analyzed using powder X-ray Diffraction (XRD) with a Rigaku SmartLab diffractometer. The samples were ground in a boron nitride mortar/pestle and loaded into 20 mm x 20 mm glass holders. A Cu Kα X-ray source with 1D silicon strip detector (D/teX™) and Ni filter Bragg Brentano geometry with 2/3 degree incident slit). Mineral fractions were estimated from Rietveld refinements performed using the Jade™ (MDI) software package. Because of the beam divergence resulting from the 2/3 degree incident slit, beam spillover during data collection occurred at angles below 20˚ 2θ, causing clay fractions to be most likely underestimated.
- X-ray Photoelectron Spectrometer (XPS) (Kratos AXIS-UltraDLD) was used to acquire the near surface (5-10 nm) elemental composition and oxidation states. Monochromatic Al K $\alpha$ source operating at 225W was used. Survey spectra were acquired at 80 eV and high resolution at 20 eV pass energy. The data obtained are the average of 3 different areas per sample. Charge compensation was accomplished using low energy electrons at standard operating conditions of -3.1 V bias voltage, 1.0 V filament voltage and filament current of 2.1 A. Gold powder was deposited on each sample, and Au 4f spectra were acquired for calibration purposes. All spectra processing was done in CasaXPS. Atomic percentage content was calculated using sensitivity factors provided by the manufacturer. All the spectra were charge referenced to Au 4f at 84 eV. A 70% Gaussian/ 30% Lorentzian (GL (30)) line shape was used for the curve-fits.

- Scanning Transmission Electron Microscopy (STEM) was used to characterize the fine-grained mineralogy of sediment and suspended sediment samples. STEM analysis was performed using a JEOL 2010F FEGTEM/STEM operating at 200 kV. Samples of sediment and suspended sediment in water were dropped using a pipette onto standard holey carbon film-covered Cu TEM grids. The water was allowed to evaporate in air and then the dry samples were studied in the TEM. High-angle annular dark-field (HAADF) images of the samples were obtained and then representative areas of the sample were studied using STEM X-ray mapping. An Oxford Instruments Aztec Energy Dispersive Spectroscopy (EDS) analysis system coupled to an $XMax^N$ 80 $mm^2$ EDS detector was used to obtained full spectral X-ray maps of the sample. After collection of the maps, EDS X-ray spectra for individual mineral phases were extracted from the data cube by drawing regions of interest around distinct mineral grains based on the HAADF images. This approach allows integration of X-ray counts from multiple pixels to be obtained enabling concentrations of minor elements to be detected much more effectively.
- The samples for Mössbauer spectroscopy was prepared by sealing the bulk sediment between two pieces of polyimide tape, taking care that the total sample absorption was similar to that of a 7 μm Fe(0) foil. The $^{57}$Fe Mössbauer spectra were collected in transmission mode with a constant acceleration drive system (SEE Co., Inc) and a $^{57}$Co(Rh) source. Samples were mounted in a Janis gas-exchange closed cycle cryostat capable of maintaining a sample temperature of 17.5K. The Mössbauer source was at room temperature. Data were calibrated with an α-Fe foil at room temperature. Spectral fitting was done with the Recoil software package[10] using Voigt lineshapes with a Lorentzian line width fixed to that of the instrumentally-determined width of the inner

lines of the Fe foil (0.13 mm/s). Unless otherwise noted spectra are fitted with all parameters allowed to float during the fitting routine. Quadrupole shift parameters are reported as 2ε, which is twice the parameter epsilon_0 in Recoil.

**References**


(1) van der Zee, C.; Roberts, D. R.; Rancourt, D. G.; Slomp, C. P., Nanogoethite is the dominant reactive oxyhydroxide phase in lake and marine sediments. *Geology* **2003,** *31*, 993-996.
(2) Yoshida, Y.; Langouche, G., Mössbauer Spectroscopy. *Mössbauer Spectroscopy: Tutorial Book, ISBN 978-3-642-32219-8. Springer-Verlag Berlin Heidelberg, 2013* **2013,** *1*.
(3) Murad, E.; Cashion, J., *Mössbauer Spectroscopy of Environmental Materials and their Industrial Utilization*. Kluwer Academic Publishers: 2004.
(4) Ericsson, T.; Krisnhamurthy, A.; Srivastava, B. K., Morin-Transition in Ti-Substituted Hematite: A Mössbauer Study. *Physica Scripta* **1986,** *33*, (1), 88.
(5) Dyar, M. D.; Agresti, D. G.; Schaefer, M. W.; Grant, C. A.; Sklute, E. C., Mossbauer Spectroscopy of Earth and Planetary Elements. *Annual Review of Earth and Planetary Sciences* **2006,** *34*, 83-125.
(6) Dyar, M. D.; Schaefer, M. W.; Sklute, E. C.; Bishop, J. L., Mossbauer spectroscopy of phyllosilicates: effects of fitting models on recoil-free fractions and redox ratios. *Clay Minerals* **2008,** *43*, (1), 3-33.
(7) Afanasev, A.; Gorobchenko, V.; Kulgawczuk, D.; Lukashevich, I., Nuclear γ-resonance in iron sulphates of the jarosite group. *Physica status solidi (a)* **1974,** *26*, (2), 697-701.
(8) Dutrizac, J.; Kaiman, S., Synthesis and properties of jarosite-type compounds. *The Canadian Mineralogist* **1976,** *14*, (2), 151-158.
(9) Leclerc, A., Room temperature Mössbauer analysis of jarosite-type compounds. *Physics and Chemistry of Minerals* **1980,** *6*, (4), 327-334.
(10) Lagarec, K.; Rancourt, D. G., Recoil-Mössbauer spectral analysis software for Windows, University of Ottawa, Ottawa, ON.. **1998**.

**Table S1.** Dissolved, total and suspended metal concentrations in the water samples.

| Sample location | Al (mg $l^{-1}$) | | | As (µg $l^{-1}$) | | | B (mg $l^{-1}$) | | | Ba (mg $l^{-1}$) | | |
|---|---|---|---|---|---|---|---|---|---|---|---|---|
| | Dissolved | Total | Suspended | Dissolved | Total | Suspended | Dissolved | Total | Suspended | Dissolved | Total | Suspended |
| L1 | 7.50 | 7.50 | 0.00 | 0.19 | 0.91 | 0.72 | 0.01 | 0.02 | 0.02 | -- | -- | -- |
| L2 | 0.07 | 0.10 | 0.03 | -- | 0.06 | 0.06 | -- | -- | -- | 0.00 | 0.01 | 0.00 |
| L3 | 0.06 | 2.20 | 2.14 | -- | 0.40 | 0.40 | -- | 0.01 | 0.01 | 0.00 | 0.01 | 0.01 |
| L4 | 0.07 | 0.54 | 0.47 | -- | 0.04 | 0.04 | -- | 0.00 | 0.00 | 0.01 | 0.02 | 0.00 |
| L5 | 0.04 | 0.40 | 0.36 | 0.08 | 0.16 | 0.08 | 0.04 | 0.04 | 0.00 | 0.06 | 0.07 | 0.01 |
| L6 | 0.04 | 0.46 | 0.43 | 0.17 | 0.07 | -- | 0.05 | 0.05 | -- | 0.08 | 0.09 | 0.01 |
| L7 | 0.04 | | | 0.06 | | | 0.11 | | | 0.05 | | |
| **Sample location** | **Ca (mg $l^{-1}$)** | | | **Cd (µg $l^{-1}$)** | | | **Co (µg $l^{-1}$)** | | | **Cr (µg $l^{-1}$)** | | |
| | **Dissolved** | **Total** | **Suspended** | **Dissolved** | **Total** | **Suspended** | **Dissolved** | **Total** | **Suspended** | **Dissolved** | **Total** | **Suspended** |
| L1 | 157.99 | 146.84 | -- | 1.03 | 1.03 | -- | 3.03 | 3.29 | 0.26 | 0.02 | 0.34 | 0.32 |
| L2 | 42.63 | 39.47 | -- | 0.11 | 0.14 | 0.03 | 0.10 | 0.11 | 0.01 | 0.00 | 0.18 | 0.18 |
| L3 | 59.75 | 56.24 | -- | 0.21 | 0.21 | 0.00 | 0.62 | 0.70 | 0.09 | 0.00 | 0.14 | 0.14 |
| L4 | 44.01 | 40.93 | -- | 0.07 | 0.07 | 0.00 | 0.22 | 0.22 | -- | 0.04 | 0.07 | 0.03 |
| L5 | 60.72 | 58.31 | -- | 0.01 | 0.03 | 0.02 | 0.10 | 0.14 | 0.03 | 0.15 | 0.10 | -- |
| L6 | 77.21 | 72.66 | -- | 0.02 | 0.02 | | 0.17 | 0.19 | 0.02 | 0.06 | 0.12 | 0.06 |
| L7 | 73.96 | | | 0.01 | | | 0.16 | | | 0.02 | | |
| **Sample location** | **Cu (µg $l^{-1}$)** | | | **Fe (mg $l^{-1}$)** | | | **K (mg $l^{-1}$)** | | | **Mg (mg $l^{-1}$)** | | |
| | **Dissolved** | **Total** | **Suspended** | **Dissolved** | **Total** | **Suspended** | **Dissolved** | **Total** | **Suspended** | **Dissolved** | **Total** | **Suspended** |
| L1 | 51.19 | 54.92 | 3.73 | 7.50 | 13.41 | 5.91 | 1.59 | 1.63 | 0.04 | 9.93 | 9.29 | -- |
| L2 | 0.57 | 1.89 | 1.32 | 0.02 | 0.08 | 0.06 | 0.53 | 0.55 | 0.02 | 2.86 | 2.57 | -- |
| L3 | 2.14 | 10.98 | 8.84 | 0.85 | 5.61 | 4.76 | 0.68 | 0.83 | 0.14 | 4.53 | 4.28 | -- |
| L4 | 0.59 | 2.18 | 1.59 | -- | 0.87 | 0.87 | 0.90 | 0.91 | 0.01 | 7.54 | 6.85 | -- |
| L5 | 0.72 | 1.19 | 0.47 | -- | 0.61 | 0.61 | 2.68 | 2.72 | 0.04 | 9.71 | 9.18 | -- |
| L6 | 0.64 | 1.61 | 0.96 | -- | 0.54 | 0.54 | 2.79 | 2.82 | 0.03 | 11.74 | 10.99 | -- |
| L7 | 0.88 | | | 0.02 | | | 6.22 | | | 11.78 | | |

**Table S1 *Cont.*** Dissolved, total and suspended metal concentrations in the water samples.

| Sample location | Mn (mg $l^{-1}$) | | | Mo (µg $l^{-1}$) | | | Na (mg $l^{-1}$) | | | Pb (µg $l^{-1}$) | | |
|---|---|---|---|---|---|---|---|---|---|---|---|---|
| | Dissolved | Total | Suspended | Dissolved | Total | Suspended | Dissolved | Total | Suspended | Dissolved | Total | Suspended |
| L1 | 5.79 | 5.38 | -- | 0.03 | 0.17 | 0.15 | 6.03 | 6.18 | 0.16 | 1.67 | 3.33 | 1.67 |
| L2 | 0.84 | 0.77 | -- | 0.22 | 0.23 | 0.01 | 1.85 | 2.02 | 0.16 | 0.08 | 0.41 | 0.33 |
| L3 | 1.22 | 1.15 | -- | 0.08 | 0.18 | 0.11 | 2.74 | 2.88 | 0.14 | 0.03 | 4.14 | 4.10 |
| L4 | 0.40 | 0.30 | -- | 0.07 | 0.09 | 0.02 | 2.79 | 2.88 | 0.08 | 0.05 | 0.58 | 0.53 |
| L5 | -- | 0.05 | 0.05 | 0.16 | 0.17 | 0.02 | 18.19 | 17.99 | -- | 0.13 | 0.56 | 0.43 |
| L6 | -- | 0.03 | 0.03 | 0.25 | 0.21 | -- | 30.85 | 30.01 | -- | 2.21 | 0.39 | -- |
| L7 | 0.00 | | | 0.23 | | | 52.57 | | | 0.15 | | |

| Sample location | U (µg $l^{-1}$) | | | Si (mg $l^{-1}$) | | | Sr (µg $l^{-1}$) | | | V (µg $l^{-1}$) | | |
|---|---|---|---|---|---|---|---|---|---|---|---|---|
| | Dissolved | Total | Suspended | Dissolved | Total | Suspended | Dissolved | Total | Suspended | Dissolved | Total | Suspended |
| L1 | 0.16 | 0.11 | -- | 13.61 | 12.24 | -- | 213.39 | 220.48 | 7.09 | 0.02 | 0.80 | 0.79 |
| L2 | 0.04 | 0.15 | 0.11 | 3.21 | 2.80 | -- | 41.77 | 40.93 | -- | 0.00 | 0.13 | 0.13 |
| L3 | 0.01 | 0.13 | 0.12 | 5.30 | 5.25 | -- | 70.71 | 75.29 | 4.58 | 0.00 | 0.34 | 0.34 |
| L4 | 0.05 | 0.10 | 0.05 | 3.60 | 3.40 | -- | 38.42 | 37.55 | -- | 0.01 | 0.11 | 0.10 |
| L5 | 0.14 | 0.15 | 0.01 | 2.92 | 3.07 | 0.15 | 77.32 | 80.02 | 2.70 | 0.06 | 0.17 | 0.12 |
| L6 | 0.21 | 0.25 | 0.04 | 2.11 | 2.54 | 0.43 | 123.14 | 128.51 | 5.37 | 0.07 | 0.22 | 0.15 |
| L7 | 0.17 | | | 3.18 | | | 115.82 | | | 0.10 | | |

| Sample location | Zn (mg $l^{-1}$) | | |
|---|---|---|---|
| | Dissolved | Total | Suspended |
| L1 | 3.55 | 2.94 | -- |
| L2 | 0.26 | 0.21 | -- |
| L3 | 0.60 | 0.54 | -- |
| L4 | 0.09 | 0.13 | 0.04 |
| L5 | -- | -- | -- |
| L6 | -- | -- | -- |
| L7 | -- | | |

**Table S2.** Summary of data collected from the Animas River.

| Sample ID | Site description | Elevation (ft) | T[1] ($^{o}$C) | DO[2] (mg $l^{-1}$) | SC[3] ($\mu$S $cm^{-1}$) | pH | ORP[4] (mV) | ALK[5] (mg $l^{-1}$) |
|---|---|---|---|---|---|---|---|---|
| L1, C1 | Cement Creek 14th Street Bridge (37.8126 N, 107.6593 W) | 9315 | 7.2 | 10.3 | 1000 | 3.32 | 465.2 | 0 |
| L2 | Silverton EPA A68 Animas River Upstream of Confluence with Cement Creek (37.8110 N, 107.6589 W) | 9290 | 8.8 | 6.0 | 266.5 | 6.18 | 90.8 | 54.7 |
| L3 | Silverton EPA A72 Animas River Downstream of Confluence with Cement Creek (37.7952 N, 107.6689 W) | 9232 | 10.6 | 5.0 | 377.9 | 6.04 | 110.2 | 11.8 |
| L4 | Animas River at Baker's Bridge (37.4575 N, 107.8002 W) | 6958 | 14.0 | 5.0 | 268.3 | 7.36 | 154.4 | 55.2 |
| L5 | Animas River at Cedar Hill (36.9333 N, 107.9090 W) | 5820 | 22.4 | 6.7 | 461.8 | 8.25 | 126.4 | 141.3 |
| L6, C6 | Animas River at Farmington (36.7137 N, 108.2172 W) | 5244 | 23.8 | 3.3 | 608.0 | 8.14 | 89.0 | 161.0 |
| L7 | San Juan River Downstream of Confluence with Animas River (36.7176 N, 108.2219 W) | 5224 | 23.3 | 5.5 | 446.9 | 7.95 | 90.8 | 135.3 |

[1]T: Temperature; [2]DO: Dissolved Oxygen concentration; [3]SC: specific conductivity; [4]ORP: Oxidation-Reduction Potential; [5]ALK: Bicarbonate alkalinity

**Table S3.** Elemental composition of the Animas River sediment using X-Ray Fluorescence (XRF).

| Element ($mg\ kg^{-1}$) | Sampling locations (from North to South) | | | | | | | |
|---|---|---|---|---|---|---|---|---|
| | **C1** | **L1** | **L3** | **L4** | **L5** | **L6** | **L7** | **C6** |
| **Fluorine** | 811 | 1010 | 460 | 644 | N.D.[1] | N.D. | N.D. | N.D. |
| **Sodium** | 11142 | 1861 | 3132 | 7251 | 4493 | 7325 | 7277 | 6742 |
| **Magnesium** | 7648 | 6000 | 7891 | 6881 | 5686 | 1766 | 2413 | 3897 |
| **Aluminum** | 70836 | 86920 | 91025 | 75846 | 75092 | 46460 | 47169 | 60803 |
| **Silicon** | 314467 | 281971 | 265697 | 297395 | 294865 | 345439 | 337928 | 324284 |
| **Phosphorus** | 1622 | 3125 | 2350 | 2050 | 1350 | 600 | 562 | 984 |
| **Sulfur** | 1296 | 13750 | 5237 | 3530 | 1856 | 491 | 664 | 1029 |
| **Chlorine** | 603 | N.D. | 125 | 113 | 637 | 126 | 175 | N.D. |
| **Potassium** | 41714 | 48482 | 41041 | 40686 | 33191 | 44231 | 42539 | 37649 |
| **Calcium** | 22775 | 7991 | 9214 | 18884 | 35084 | 10002 | 12863 | 22067 |
| **Titanium** | 6483 | 10588 | 7658 | 5910 | 6953 | 3183 | 5587 | 5695 |
| **Chromium** | N.D. | 141 | N.D. | 119 | N.D. | 235 | 157 | 162 |
| **Manganese** | 2444 | 2502 | 15938 | 4833 | 2520 | 1097 | 1021 | 2390 |
| **Iron** | 61820 | 108232 | 132450 | 91624 | 71769 | 24230 | 28481 | 52575 |
| **Copper** | 139 | 686 | 590 | 319 | 211 | N.D. | N.D. | 113 |
| **Zinc** | 638 | 1485 | 3260 | 1873 | 1188 | 252 | 72 | 1009 |
| **Gallium** | N.D. | 45 | N.D. | N.D. | N.D. | N.D. | N.D. | N.D. |
| **Rubidium** | 257 | 455 | 317 | 269 | 253 | 227 | 209 | 221 |
| **Strontium** | 915 | 761 | 654 | 589 | 5250 | 335 | 345 | 459 |
| **Yttrium** | N.D. | N.D. | 192 | 120 | N.D. | 102 | 99 | 148 |
| **Zirconium** | 419 | 424 | 459 | 304 | 1393 | 384 | 3751 | 1324 |
| **Barium** | 1422 | 1017 | 1197 | 1197 | 1403 | 1442 | 1939 | 3144 |
| **Tungsten** | 167 | N.D. | N.D. | N.D. | N.D. | 163 | N.D. | N.D. |
| **Lead** | 417 | 2620 | 1552 | 968 | 531 | 72 | N.D. | 316 |
| **Niobium** | 32 | N.D. | N.D. | N.D. | N.D. | N.D. | N.D. | N.D. |

[1] N.D. Element was not detected

**Table S4.** Total metal concentrations in the sediment samples presented as the average of three aqua regia digestions and the standard deviation.

| Sampling location | mg kg$^{-1}$ | | | | | | | | | |
|---|---|---|---|---|---|---|---|---|---|---|
| | **Aluminum** | | **Arsenic** | | **Boron** | | **Barium** | | **Calcium** | |
| | Average | St. Dev. | Average | St. Dev. | Average | St. Dev. | Average | St. Dev. | Average | St. Dev. |
| C1 | 11682.4 | 273.2 | 0.54 | 0.05 | 46.1 | 1.2 | 1110.0 | 28.7 | 8371.7 | 219.1 |
| L1 | 9121.2 | 83.8 | 4.25 | 0.25 | 108.9 | 0.8 | 54.8 | 1.8 | 2401.2 | 30.9 |
| L3 | 16291.5 | 210.0 | 4.25 | 0.11 | 135.0 | 1.5 | 112.7 | 89.8 | 2811.6 | 138.1 |
| L4 | 12343.9 | 151.7 | 2.21 | 0.10 | 85.8 | 0.8 | 176.3 | 1.6 | 4310.3 | 24.4 |
| L5 | 11816.2 | 281.0 | 0.68 | 0.04 | 45.7 | 0.8 | 563.6 | 15.9 | 10612.7 | 125.1 |
| L6 | 5642.7 | 31.3 | 0.28 | 0.03 | 21.2 | 0.3 | 426.3 | 4.0 | 3250.5 | 22.7 |
| L7 | 5426.0 | 52.9 | 0.22 | 0.00 | 24.9 | 0.4 | 598.7 | 6.7 | 3797.6 | 46.7 |
| C6 | 12245.2 | 241.7 | 0.75 | 0.05 | 65.8 | 0.8 | 188.0 | 5.3 | 6682.2 | 178.4 |

| Sampling location | mg kg$^{-1}$ | | | | | | | | | |
|---|---|---|---|---|---|---|---|---|---|---|
| | **Cadmium** | | **Cobalt** | | **Chromium** | | **Copper** | | **Iron** | |
| | Average | St. Dev. | Average | St. Dev. | Average | St. Dev. | Average | St. Dev. | Average | St. Dev. |
| C1 | 0.10 | 0.01 | 0.94 | 0.04 | 2.72 | 0.16 | 8.1 | 0.4 | 21988.6 | 602.8 |
| L1 | 0.30 | 0.01 | 0.54 | 0.01 | 1.86 | 0.06 | 32.4 | 0.5 | 51314.6 | 295.4 |
| L3 | 0.66 | 0.01 | 3.20 | 0.08 | 1.34 | 0.08 | 27.0 | 0.5 | 62385.3 | 509.2 |
| L4 | 0.30 | 0.01 | 1.54 | 0.05 | 3.37 | 0.74 | 20.6 | 0.7 | 41091.3 | 453.6 |
| L5 | 0.11 | 0.00 | 0.75 | 0.02 | 1.65 | 0.04 | 5.6 | 0.2 | 22220.5 | 322.8 |
| L6 | 0.04 | 0.00 | 0.83 | 0.02 | 2.08 | 0.05 | 2.8 | 0.0 | 10365.9 | 64.2 |
| L7 | 0.04 | 0.00 | 0.85 | 0.05 | 2.49 | 0.15 | 5.3 | 0.4 | 11243.2 | 98.3 |
| C6 | 0.13 | 0.00 | 1.00 | 0.04 | 2.15 | 0.04 | 19.6 | 0.2 | 29085.1 | 568.6 |

| Sampling location | mg kg$^{-1}$ | | | | | | | | | |
|---|---|---|---|---|---|---|---|---|---|---|
| | **Potassium** | | **Lithium** | | **Magnesium** | | **Manganese** | | **Molybdenum** | |
| | Average | St. Dev. | Average | St. Dev. | Average | St. Dev. | Average | St. Dev. | Average | St. Dev. |
| C1 | 2756.6 | 58.7 | 6.1 | 0.2 | 2881.2 | 77.7 | 843.8 | 21.8 | 0.17 | 0.01 |
| L1 | 3385.7 | 19.8 | 13.2 | 0.7 | 3184.6 | 22.6 | 598.8 | 4.4 | 1.12 | 0.03 |
| L3 | 3152.2 | 522.1 | 18.3 | 3.9 | 5122.8 | 42.3 | 6555.5 | 53.8 | 1.00 | 0.02 |
| L4 | 3261.8 | 31.6 | 15.4 | 4.1 | 4840.6 | 48.6 | 2383.9 | 25.6 | 0.63 | 0.09 |
| L5 | 2083.0 | 59.8 | 21.0 | 0.2 | 3194.4 | 49.3 | 883.8 | 11.2 | 0.18 | 0.00 |
| L6 | 1689.9 | 4.7 | 9.3 | 0.5 | 1310.9 | 7.0 | 443.8 | 3.0 | 0.09 | 0.00 |
| L7 | 1508.9 | 15.5 | 8.7 | 0.1 | 1232.2 | 12.5 | 257.9 | 2.6 | 0.09 | 0.00 |
| C6 | 3278.3 | 74.9 | 25.1 | 0.2 | 6213.8 | 119.1 | 1028.3 | 22.5 | 0.23 | 0.00 |

**Table S4** ***Cont.*** Total metal concentrations in the sediment samples presented as the average of three aqua regia digestions and the standard deviation.

| Sampling location | mg kg$^{-1}$ | | | | | | | | | |
|---|---|---|---|---|---|---|---|---|---|---|
| | Sodium | | Nickel | | Lead | | Silicon | | Strontium | |
| | Average | St. Dev. | Average | St. Dev. | Average | St. Dev. | Average | St. Dev. | Average | St. Dev. |
| C1 | 444.9 | 11.3 | 5.1 | 0.2 | 10.0 | 0.4 | 41.5 | 13.3 | 5.4 | 0.2 |
| L1 | 147.3 | 1.2 | | | 108.4 | 1.8 | 32.8 | 1.2 | 20.8 | 0.7 |
| L3 | 192.0 | 14.7 | 4.7 | 1.5 | 59.5 | 1.3 | 17.2 | 3.4 | 5.4 | 0.2 |
| L4 | 392.1 | 2.7 | 6.7 | 0.6 | 40.8 | 1.4 | 27.7 | 12.6 | 6.1 | 0.2 |
| L5 | 456.8 | 4.0 | 4.5 | 2.2 | 9.2 | 0.3 | 45.5 | 11.6 | 6.9 | 1.0 |
| L6 | 410.0 | 1.9 | 2.7 | 0.2 | 2.2 | 0.1 | 26.6 | 3.1 | 3.1 | 0.1 |
| L7 | 545.5 | 6.4 | 3.5 | 0.1 | 0.8 | 0.0 | 26.4 | 5.6 | 2.9 | 0.1 |
| C6 | 732.4 | 17.3 | 3.3 | 0.1 | 14.9 | 1.3 | 27.4 | 8.9 | 5.3 | 0.2 |

| Sampling location | mg kg$^{-1}$ | | | | | | µg kg$^{-1}$ | |
|---|---|---|---|---|---|---|---|---|
| | Uranium | | Vanadium | | Zinc | | Mercury | |
| | Average | St. Dev. | Average | St. Dev. | Average | St. Dev. | Average | St. Dev. |
| C1 | 0.14 | 0.00 | 3.3 | 0.1 | 431.6 | 11.2 | 23.6 | 1.5 |
| L1 | 0.10 | 0.00 | 3.6 | 0.1 | 729.6 | 5.7 | 86.7 | 3.0 |
| L3 | 0.22 | 0.01 | 4.3 | 0.1 | 1385.6 | 16.3 | 73.6 | 0.9 |
| L4 | 0.28 | 0.04 | 4.7 | 0.2 | 807.0 | 7.6 | 44.6 | 0.3 |
| L5 | 0.13 | 0.00 | 2.8 | 0.1 | 382.8 | 2.6 | 27.9 | 0.7 |
| L6 | 0.07 | 0.00 | 1.3 | 0.0 | 96.2 | 0.2 | 5.3 | 0.0 |
| L7 | 0.15 | 0.01 | 1.6 | 0.1 | 16.7 | 1.7 | 14.2 | 1.3 |
| C6 | 0.12 | 0.00 | 4.6 | 0.1 | 287.8 | 7.7 | 15.7 | 0.7 |

**Table S5.** Metal speciation in the sediments using X-ray photoelectron spectroscopy (XPS).

| Sampling locations | % Content | | | | | | | | | | | |
|---|---|---|---|---|---|---|---|---|---|---|---|---|
| | C 1s | O 1s | Si 2p | Na 2s | Mg 2p | Fe 3p | Mn 2p | Pb 4f | Zn 2p | P 2p | S 2p | N 1s |
| **C1** | 22.7 | 56.1 | 16.3 | 0.5 | 2.0 | 1.3 | 0.11 | --- | 0.03 | 0.10 | --- | 0.8 |
| **L1** | 23.6 | 57.4 | 13.9 | 0.1 | 0.8 | 2.3 | 0.05 | 0.04 | 0.01 | 0.25 | 0.65 | 0.8 |
| **L4** | 29.7 | 52.3 | 13.3 | 0.4 | 1.1 | 2.0 | 0.19 | 0.02 | 0.08 | 0.00 | 0.17 | 0.7 |
| **L7** | 23.1 | 54.9 | 17.5 | 1.0 | 0.8 | 1.5 | --- | --- | --- | 0.15 | 0.00 | 1.3 |

| Sampling locations | % Content | | | | | | | | | |
|---|---|---|---|---|---|---|---|---|---|---|
| | $Fe^{2+}$ | $Fe^{3+}$ | Pb | PbO | $SO_4^{2-}$ | $PO_4^{3-}$ | Amide | $NH_3$ | $N\text{-}O_2$ | $N\text{-}O_3$ |
| **C1** | 64.0 | 36.0 | --- | --- | --- | 100.0 | 70.2 | 29.8 | --- | --- |
| **L1** | 75.9 | 24.1 | 0.0 | 100.0 | 100.0 | 100.0 | 76.6 | 23.4 | --- | --- |
| **L4** | 76.3 | 23.7 | 17.8 | 82.2 | 100.0 | 0.0 | 45.6 | 10.3 | --- | --- |
| **L7** | 12.0 | 88.0 | --- | --- | --- | 100.0 | 95.0 | 5.0 | 9.8 | 34.3 |

**Table S6** Summary of the mineral weight distribution in samples L1 and L4 obtained by XRD, and the refinement statistics of the method used.

| Phase | L1 Weight % (ESD)[a] | L4 Weight % (ESD) |
|---|---|---|
| Quartz | 37.1 (3.1) | 36.8 (3.0) |
| Illiite | 29.9 (3.3) | 12.1 (5.3) |
| Albite | 7.3 (0.8) | 17.6 (1.7) |
| Chlorite | 17.6 (2.0) | 10.7 (1.6 |
| Clinoptolite | --- | 5.6 (0.9) |
| Microcline | --- | 14.7 (2.3) |
| Zeolite | --- | 2.6 (0.3) |
| Hydronium Jarosite | 7.4 (1.7) | --- |
| **Refinement statistics** | **L1** | **L4** |
| R[b] | 13.57% | 12.51% |
| E[c] | 11.08% | 11.10% |
| R/E | 1.22 | 1.13 |

[a]ESD: Estimated standard deviations.

[b]R: R-factor = square root of the quantity minimized, scaled by the weighted intensities

[c]E: “best posible” or “expected” R-factor

**Table S7.** Mössbauer spectral parameters derived from fitting Animas River samples C1, L1 and L4.

| T (K) | Component | Relative area (%)[a] | Center shift, CS (mm/s) | Quadrupole splitting, QS or 2ε[b] (mm/s) | σ(Δ)[c] (mm/s) | Hyperfine field, H (Tesla) | σ(H)[d] (Tesla) | $\chi_v^2$ |
|---|---|---|---|---|---|---|---|---|
| **Sample C1** | | | | | | | | |
| 77 | $Fe^{3+}$ doublet 1 | 13.4 (1.0) | 0.49 (0.01) | 0.62 | 0.27 | - | - | 0.99 |
| | $Fe^{3+}$ doublet 2 | 6.7 (1.2) | 0.50 (0.02) | 1.76 | 0.38 | - | - | |
| | $Fe^{2+}$ doublet | 22.4 (0.6) | 1.27 (0.00) | 2.85 | 0.19 | - | - | |
| | goethite | 41.6 (1.0) | 0.50 (0.01) | -0.22 | - | 41.2 | 15.0 | |
| | hematite | 16.0 (1.2) | 0.48 (0.01) | -0.15 | - | 53.2 | 0.7 | |
| 17.5 | $Fe^{3+}$ doublet 1 | 9.8 (1.0) | 0.49 (0.02) | 0.64 | 0.30 | - | - | 0.95 |
| | $Fe^{3+}$ doublet 2 | 5.6 (0.9) | 0.55 (0.02) | 1.83 | 0.28 | - | - | |
| | $Fe^{2+}$ doublet | 22.2 (1.2) | 1.27 (0.00) | 2.83 | 0.18 | - | - | |
| | goethite | 51.1 (2.6) | 0.49 (0.01) | -0.20 | - | 53.4 | 0.52 | |
| | hematite | 11.4 (2.8) | 0.51 (0.01) | -0.14 | - | 45.1 | 14.0 | |
| **Sample L1** | | | | | | | | |
| 270 | $Fe^{3+}$ doublet 1 | 40.7 (5.2) | 0.37 (0.01) | 0.59 | 0.15 | - | - | 0.59 |
| | $Fe^{3+}$ doublet 2 | 21.3 (5.3) | 0.38 (0.17) | 1.13 | 0.18 | - | - | |
| | $Fe^{2+}$ doublet | 6.7 (1.2) | 1.14 (0.55) | 2.64 | 0.19 | - | - | |
| | collapsed sextet | 31.2 (3.7) | 0.42 (0.20) | -0.24[e] | - | 25.0 | 13.3 | |
| 77 | $Fe^{3+}$ doublet | 35.7 (0.8) | 0.46 (0.01) | 0.88 | 0.38 | - | - | 1.27 |
| | $Fe^{2+}$ doublet | 5.6 (0.5) | 1.24 (0.01) | 2.88 | 0.13 | - | - | |
| | goethite | 58.7 (0.9) | 0.47 (0.01) | -0.24 | - | 36.1 | 16.8 | |
| 17.5 | $Fe^{3+}$ doublet | 6.2 (0.7) | 0.43 (0.02) | 0.76 | 0.37 | - | - | 1.26 |
| | $Fe^{2+}$ doublet | 6.6 (0.5) | 1.26 (0.01) | 2.84 | 0.22 | - | - | |
| | goethite | 17.2 (2.4) | 0.50 (0.01) | -0.22 | - | 49.7 | 0.85 | |
| | nano-goethite + jarosite | 69.9 (2.3) | 0.48 (0.01) | -0.19 | - | 40.9 | 11.6 | |
| **Sample L4** | | | | | | | | |
| 270 | $Fe^{3+}$ doublet 1 | 25 (11) | 0.40 (0.01) | 0.54 | 0.11 | - | - | 0.69 |
| | $Fe^{3+}$ doublet 2 | 35 (10) | 0.35 (0.01) | 1.01 | 0.30 | - | - | |
| | $Fe^{2+}$ doublet | 15.6 (3.1) | 1.21 (0.03) | 2.54 | 0.18 | - | - | |
| | hematite | 6.3 (1.9) | 0.39 (0.05) | -0.23 | - | 51.1 | 1.3 | |
| | collapsed sextet | 18.7 (4.5) | 0.42[e] | -0.24[e] | - | 20.7 | 14.3 | |
| 77 | $Fe^{3+}$ doublet | 39.7 (1.1) | 0.49 (0.00) | 0.83 | 0.35 | - | - | 0.95 |
| | $Fe^{2+}$ doublet | 13.2 (0.6) | 1.24 (0.01) | 2.88 | 0.21 | - | - | |
| | goethite | 44.9 (1.3) | 0.49 (0.02) | -0.24 | - | 34.1 | 17.1 | |
| | hematite | 2.2 (0.9) | 0.52 (0.04) | -0.15 | - | 53.0 | 0.003 | |
| 17.5 | $Fe^{3+}$ doublet | 9.1 (1.7) | 0.47 (0.02) | 0.84 | 0.39 | - | - | 1.03 |
| | $Fe^{2+}$ doublet | 13.6 (0.5) | 1.26 (0.01) | 2.82 | 0.22 | - | - | |
| | goethite | 5.8 (1.6) | 0.51 (0.1) | -0.26 | - | 49.5 | 0.58 | |
| | nano-goethite + jarosite | 69.8 (1.5) | 0.47 | -0.20 | - | 38.4 | 13.8 | |
| | hematite | 1.7 (0.7) | 0.53 (0.04) | -0.12 | - | 53.3 | 0.33 | |

[a] value in parenthesis reflects the error (1σ) in determination of the relative area for each component
[b] 2ε = quadrupole shift parameter in sextet
[c] σ(Δ) = standard deviation of quadrupole splitting component
[d] σ(H) = standard deviation of hyperfine field component
[e] = parameter held constant during fitting

**Table S8.** Mössbauer spectral parameters derived from fitting the synthetic K-jarosite.

| Temp. (K) | Component | Relative area (%) | Center shift, CS (mm/s) | Quadrupole splitting, QS or 2ε [b] (mm/s) | σ(Δ) [c] (mm/s) | Hyperfine field, H (Tesla) | σ(H) [d] (Tesla) | $\chi_v^2$ |
|---|---|---|---|---|---|---|---|---|
| 295 | doublet | 100 | 0.38 (0.00) | 1.11 | 0.39 | - | - | 0.70 |
| 77 | doublet | 100 | 0.49 (0.00) | 1.14 | 0.27 | - | - | 1.42 |
| 19 | sextet | 100 | 0.49 (0.01) | -0.158 | - | 42.4 | 9.1 | 1.28 |

[a] value in parenthesis reflects the error (1σ) in determination of the relative area for each component
[b] 2ε = quadrupole shift parameter in sextet
[c] σ(Δ) = standard deviation of quadrupole splitting component
[d] σ(H) = standard deviation of hyperfine field component

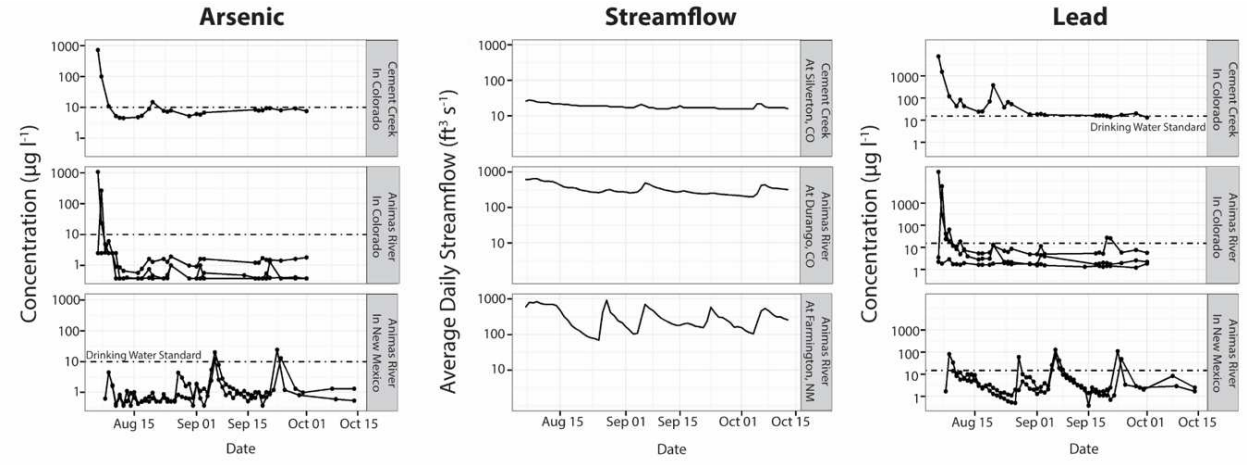


**Figure S1.** Arsenic and Pb concentrations (suspended metal) in surface water from August 5 to October 14, 2015, in Colorado and New Mexico. Peaks in total metal concentrations occurred following high-flow events, as shown in the streamflow hydrograph. Total metal concentrations were obtained from the EPA website[21] and streamflow data were downloaded from the US Geological Survey National Water Information System website.[22]

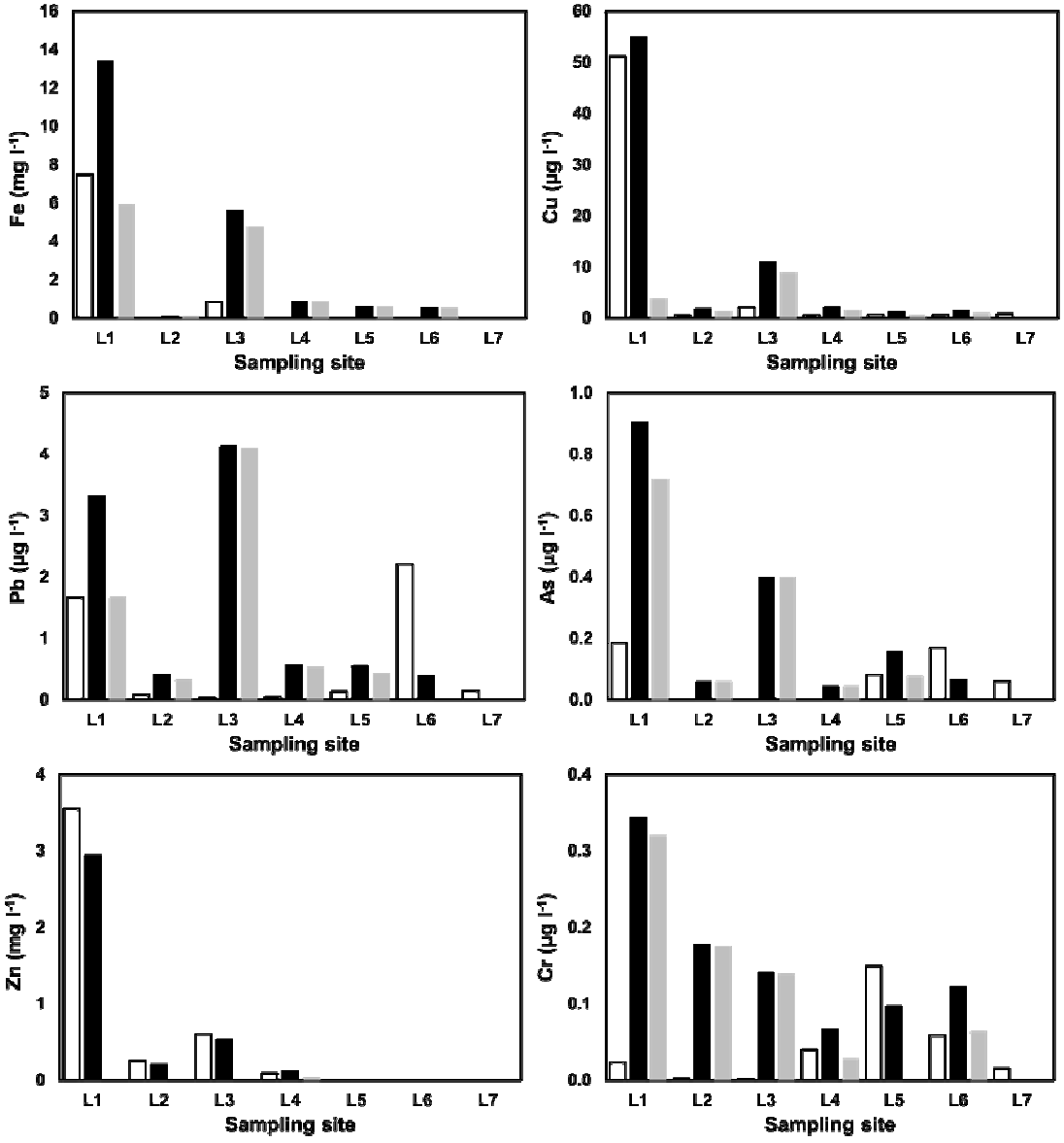


**Figure S2.** Selected metal concentrations in water samples. The graphs differentiate between the dissolved metal concentration (empty bar), total metal concentration (black bar), and the suspended metal concentration (grey bar).

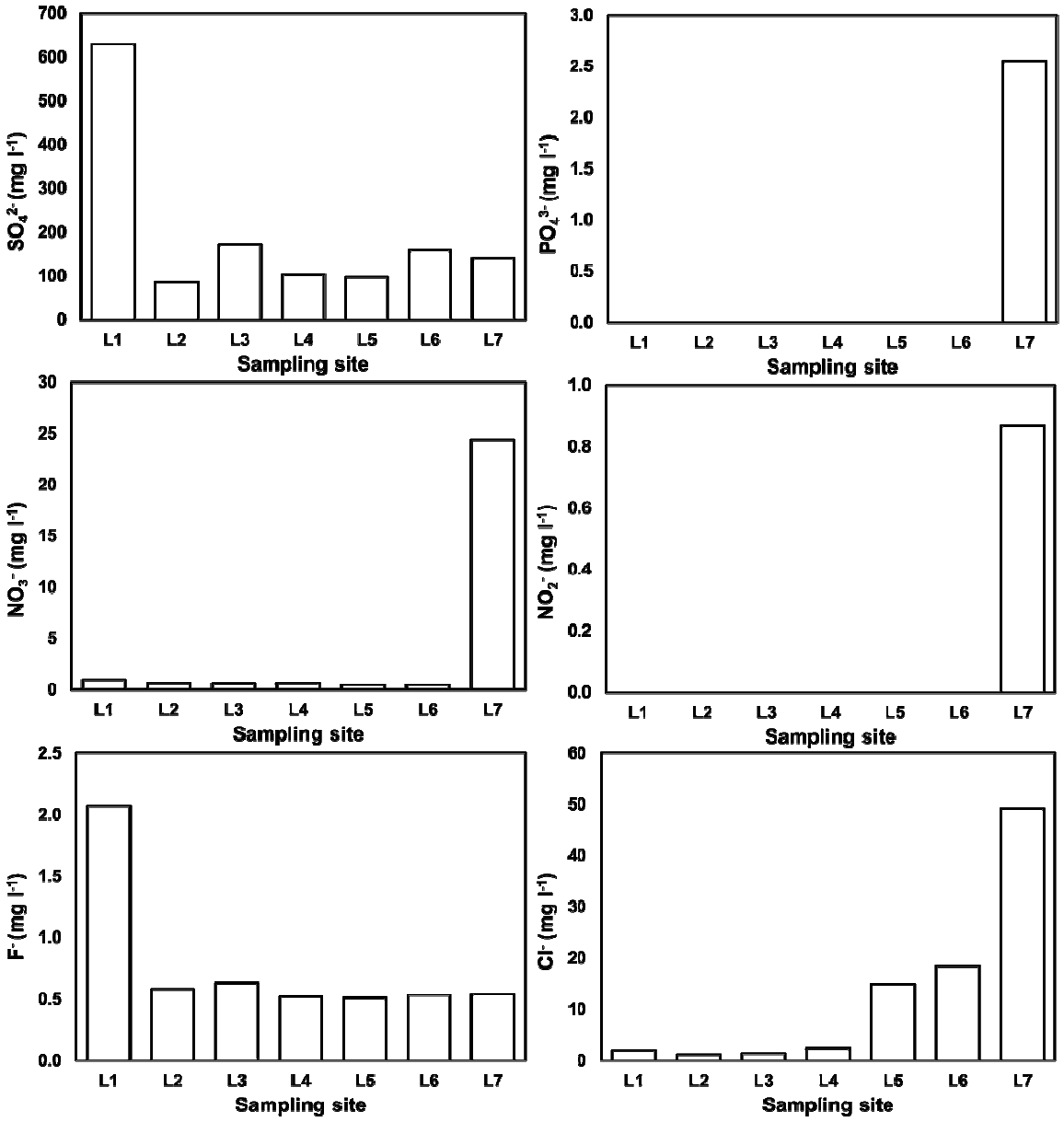


**Figure S3.** Concentrations of the ions in the water sample at the different sampling locations.

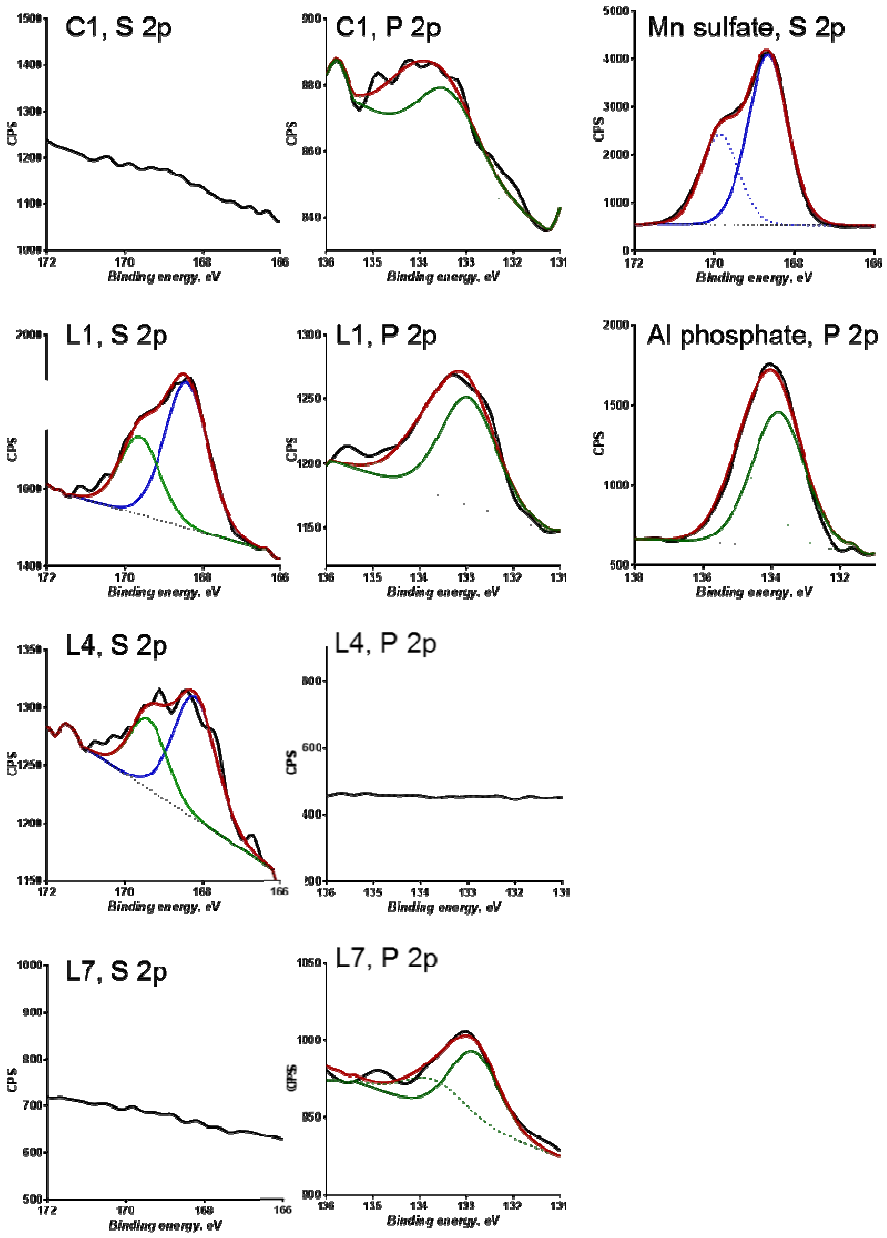


**Figure S4.** X-ray photoelectron spectra (XPS) of sulfur (S) and phosphorous (P) for the sediment samples C1, L1, L4 and L7. The figure includes the XPS of $MnSO_4$ and $Al_3PO_4$ (Ref.) for comparison with the sediment samples.

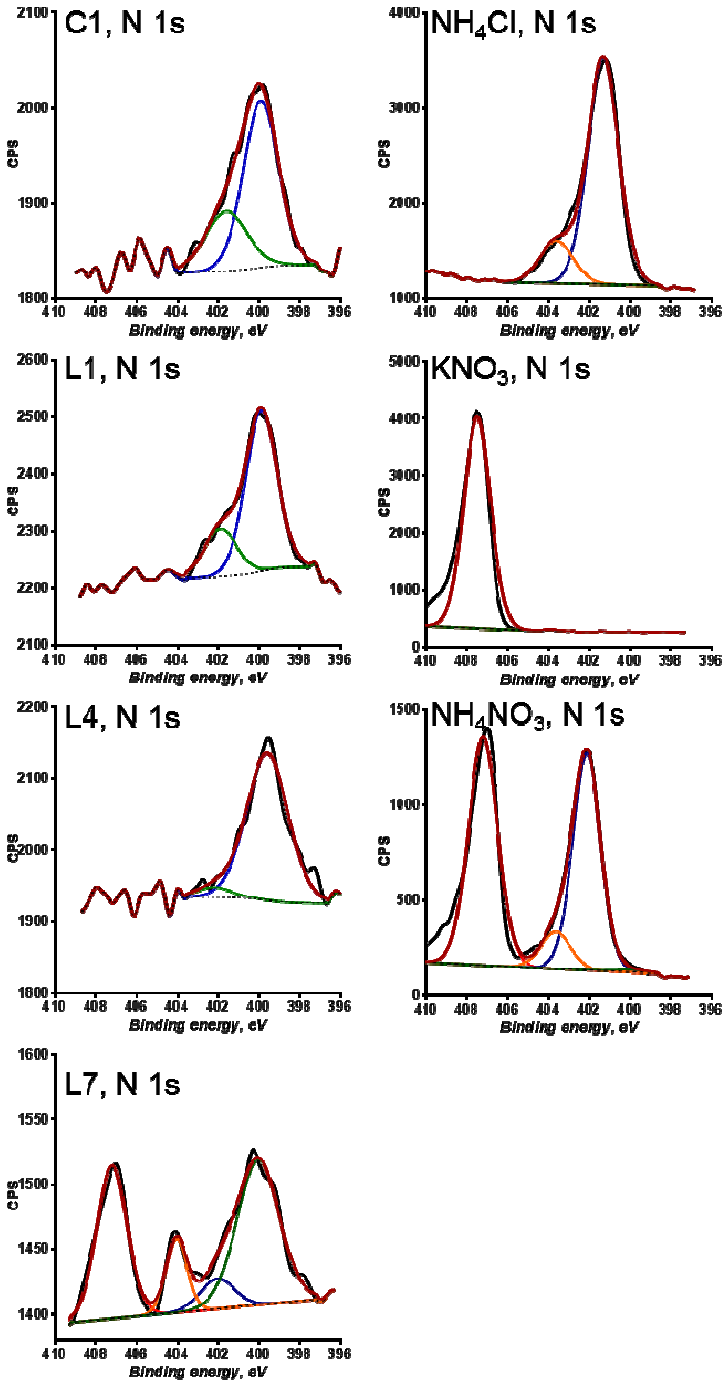


**Figure S5.** X-ray photoelectron spectra (XPS) of nitrogen (N) for the sediment samples C1, L1, L4 and L7. The figure includes the XPS of $NH_4Cl$, $KNO_3$ and $NH_4NO_3$ (Ref.) for comparison with the sediment samples.

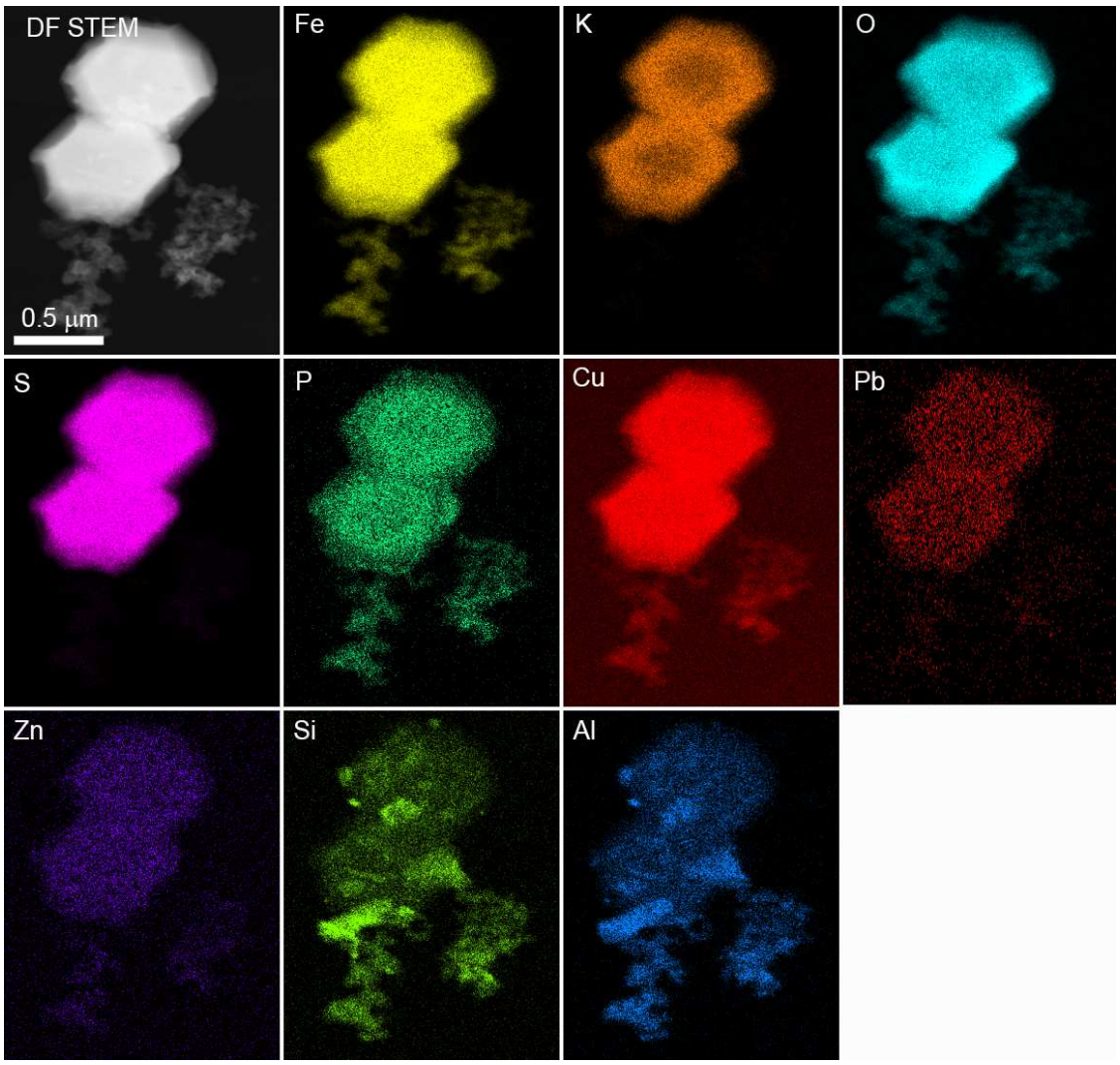


**Figure S6.** Scanning transmission electron microscope (STEM) and STEM X-ray map data of Pb-bearing jarosite crystals in sediment sample from Baker's Bridge near Hermosa, L4. Upper left image is a dark-field STEM image showing two submicron, euhedral crystals of jarosite (bright in the image), associated with fine-grained, clay-rich material and Fe-oxyhydroxides (lower part of the image). Additional images show STEM X-ray maps for Fe, K, O, S, P, Cu, Pb, Zn, Si and Al. The intensity of the color is correlated with the concentration of the element in the sample. The data show that in addition to the major elements, Fe, K, Cu, O, and S, the jarosite grains also contain detectable concentrations of P, Pb and Zn. The variations in X-ray intensity for K and P suggest that there may be some compositional zoning in the jarosite grains. The Si and Al X-ray maps show that silicate material is present adhering to the jarosite.

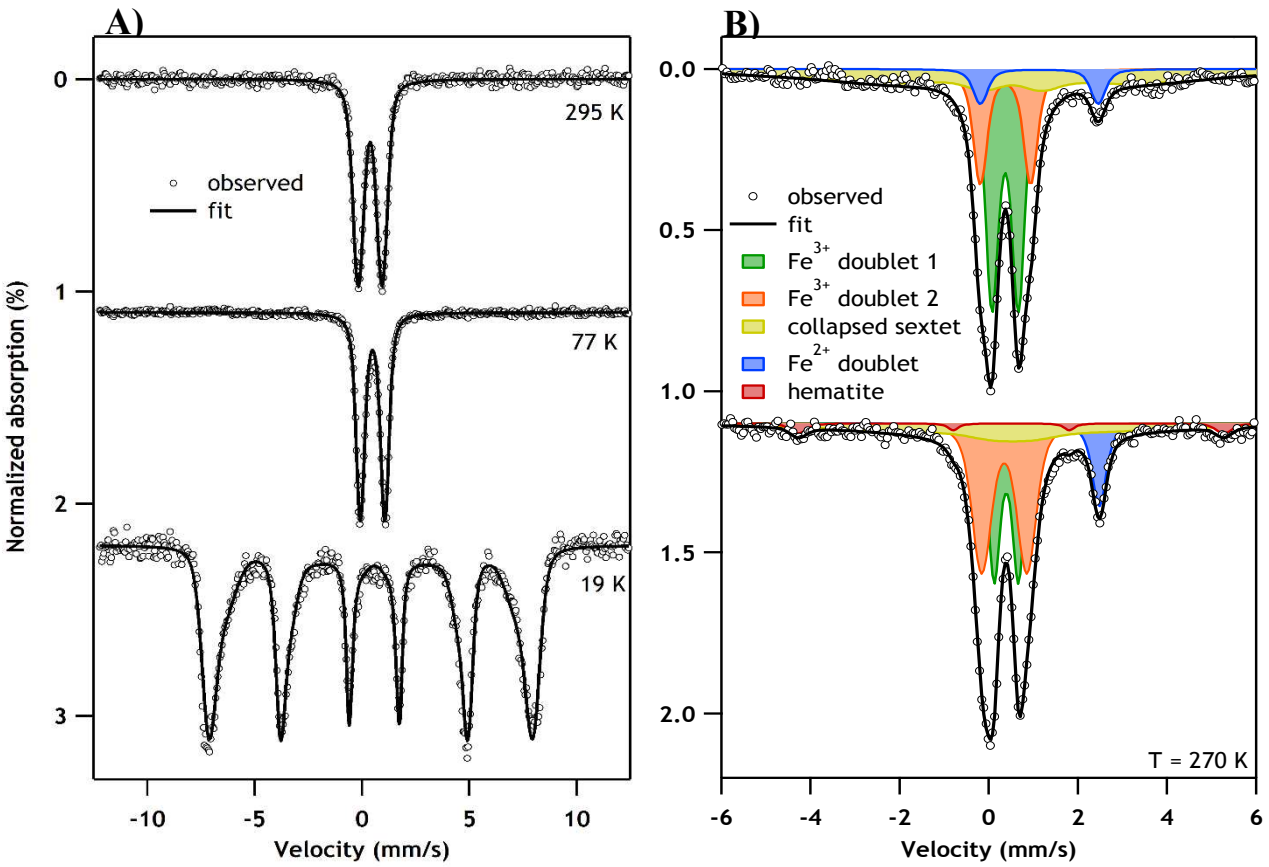


**Figure S7.** Mössbauer spectra: Panel A: $^{57}$Fe-Mössbauer spectra of synthetic K-jarosite collected at 295 K, 77 K and 19 K, shown with spectral fits (Table S7). Panel B: Mössbauer spectra collected at a temperature of 270 K for samples L1 (top) and L4 (bottom), with spectral fits shown. Mössbauer hyperfine parameters are reported in Table S6.